Microstructure evolution and mechanical response-based shortening of thermal post-treatment for electron beam melting (EBM) produced Alloy 718

Materials Science & Engineering A 820 (2021) 141515

Contents lists available at ScienceDirect

Materials Science & Engineering A

journal homepage: www.elsevier.com/locate/msea

Microstructure evolution and mechanical response-based shortening of thermal post-treatment for electron beam melting (EBM) produced Alloy 718

Sneha Goel [a,*], Enrico Zaninelli [b], Tejas Gundgire [a], Magnus Ahlfors [c], Olanrewaju Ojo [d], Uta Klement [e], Shrikant Joshi [a]

[a] Department of Engineering Science, University West, 46186 Trollhättan, Sweden
[b] Department of Engineering Enzo Ferrari, University of Modena and Reggio Emilia, 41100 Modena, Italy
[c] Quintus Technologies AB, 721 66 Västerås, Sweden
[d] Department of Mechanical Engineering, University of Manitoba, Winnipeg, R3T 5V6, Canada
[e] Department of Industrial and Material Science, Chalmers University of Technology, 41296 Gothenburg, Sweden

ARTICLE INFO

Keywords:
Additive manufacturing
Electron beam melting
Alloy 718
Post-treatment
Microstructure evolution
Mechanical properties

ABSTRACT

Electron beam melting (EBM) produced Alloy 718 was subjected to thermal post-treatment involving hot isostatic pressing (HIPing) and heat treatment (HT). Subjecting the material to HIPing at 1120 °C led to significant densification. Study of microstructure evolution during HT (comprising of solution treatment and aging) showed possibility of significantly shortening the HT duration, particularly the time for two-step aging from the standard (8 h + 8 h) long cycle to possibly a shortened (4 h + 1 h) cycle. Another approach for shortening the post-treatment cycle by integrating the HIPing with HT inside the HIP vessel was also successfully implemented. The above observations were further substantiated by tensile response of the material subjected to the varied post-treatment cycles; out of all the post-treatments steps, tensile behaviour was observed to be mainly affected by the aging treatment. Further prospects for shortening the post-treatment protocol are also described, such as shortening of HIPing duration for the typical 4 h to 1 h cycle as well as possible elimination of solution treatment step from the entire post-treatment protocol specifically when prior HIPing is performed. Heat treatment with prior HIPing was found to be crucial for improving fatigue life, because subjecting EBM Alloy 718 to only HT, irrespective of the short or standard long protocol, rendered inferior fatigue response.

1. Introduction

Electron beam melting (EBM), which is one of the growing additive manufacturing (AM) techniques [1], is capable of producing complex geometries in layer-by-layer fashion. Given the layer thickness of 50–200 μm [2] the part design can be greatly customized. The high powder bed temperature during EBM is beneficial in avoiding significant residual stress formation, unlike that commonly observed during laser powder bed fusion (LPBF) processing. Electron beam melting has been used to produce geometries with different types of materials, such as Ti-based alloys, Co-based superalloys, Ni-based superalloys, etc. [3,4]. Alloy 718, also known as Inconel 718, which is a precipitation hardened Ni (and Fe)-based superalloy was used in this study. Alloy 718 particularly is an important candidate to process by use of EBM owing to its workhorse status in the aerospace engine sector in addition to its various applications in oil and gas sector, nuclear industry etc. Due to the processing conditions that prevail, defects are typically formed in EBM built Alloy 718. These defects have been known to be responsible for reducing fatigue life [5] and introducing anisotropy [6] in this material. Moreover, due to the segregation of the alloying elements, particularly Nb, in the interdendritic region during solidification together with high powder bed temperature, the as-built microstructure can exhibit large amounts of δ phase precipitates [7]. Therefore, it is important to control the microstructure and consequently the mechanical behaviour of EBM Alloy 718 through appropriate post-processing thermal treatments (henceforth referred merely as post-treatments).

Notwithstanding the above, there is no reported systematic effort on investigating the influence of various post-treatments, such as hot

* Corresponding author.
E-mail address: sneha.goel@psi.ch (S. Goel).

https://doi.org/10.1016/j.msea.2021.141515
Received 26 January 2021; Received in revised form 5 May 2021; Accepted 5 May 2021
Available online 28 May 2021

Table 1
Nominal chemical composition of the Alloy 718 powder utilized in the EBM process.

Element	Ni	Cr	Fe	Nb	Mo	Ti	Al	C	N	O
wt.%	51.67	19.09	Rem.	5.31	3.12	0.89	0.53	0.04	0.02	0.02

isostatic pressing (HIPing) and heat treatment (HT) on EBM Alloy 718. The application of HIPing at typically 1200 °C with subsequent HT has shown to yield significantly improved fatigue and stress rupture life of EBM Alloy 718 [5,8]. However, the use of such high temperature for HIPing is also associated with grain growth [9]. Suppression of grain coarsening is crucial to preserve mechanical properties of the material, and it demands careful control of the parameters during HIPing, particularly temperature and time [1]. The commonly observed choice of a temperature of 1200 °C for HIPing appears to be borrowed from the typical practice for cast Alloy 718 [10]. Moreover, the HT employed after HIPing also appears to be directly borrowed from what has been traditionally employed for conventionally produced (cast/wrought) Alloy 718. This choice is also reflected in the ASTM F3055 standard for powder bed fusion produced Alloy 718, which recommends solution treatment (ST) for nearly 1 h and two-step aging for 18–20 h [11]; these are typically applied for precipitation of δ phase and strengthening precipitates, respectively. However, it is well known that the microstructure of an EBM Alloy 718 is distinctly different from that resulting through conventional processing routes. For instance, the size of defects, grains and segregations in an EBM Alloy 718 are much finer than those typically encountered in castings [6,12,13].

Therefore, there might be possibility to reduce the above long time for HT for EBM Alloy 718 by systematically studying microstructure evolution during the duration of conventional HT. For instance, the duration for aging determines the size of the strengthening precipitates formed during aging, and the latter influences the strength of Alloy 718 [14]. In the context of mechanical strength it is worth elaborating that the strength of Alloy 718 is dependent on several contributing factors such as, grain boundary strengthening, precipitation strengthening, solid solution strengthening, and work hardening [15–18]. Among these, precipitation strengthening is the most crucial factor for Alloy 718. Precipitation strengthening in Alloy 718 is provided by the γ" and γ′ phases, where the γ" phase is the major strengthening phase because it produces significant coherency strains due to large lattice mismatch with the matrix, on the order of 2.9% [19]. In addition, γ′ phase also provides minor coherency strengthening in Alloy 718 matrix (~0.1% lattice mismatch with the matrix) [19]. In addition to coherency strain hardening, the γ"/γ′ phases also strengthen the material through order strengthening [20].

While there have been several studies on microstructure evolution during aging of conventionally produced Alloy 718, a majority of them have involved one-step treatments [14,21–24]. A recently published research on LPBF Alloy 718 involving study of microstructure evolution during one-step aging treatment discusses the possibility of shortening the aging duration [25]. However, aging of Alloy 718 is typically carried out in two-stages particularly for gas turbine applications, i.e., Age1 at higher temperature followed by Age2 at lower temperature [26]. It should also be mentioned that precipitation of strengthening precipitates γ"/γ′ is quite complex which is also reflected in the diverse reported findings in the literature, for instance on the microstructure evolution behaviour of these precipitates during aging. This complexity possibly arises due to the sensitivity of precipitation characteristics on the precise starting state of the material [15,27,28]; no detailed study on precipitate evolution during two-step aging of EBM Alloy 718 has been reported.

To the best of the authors' knowledge, the present study is the first reported systematic effort on investigating individual effect of each of the thermal post-treatment steps, involving HIPing, ST and two-step

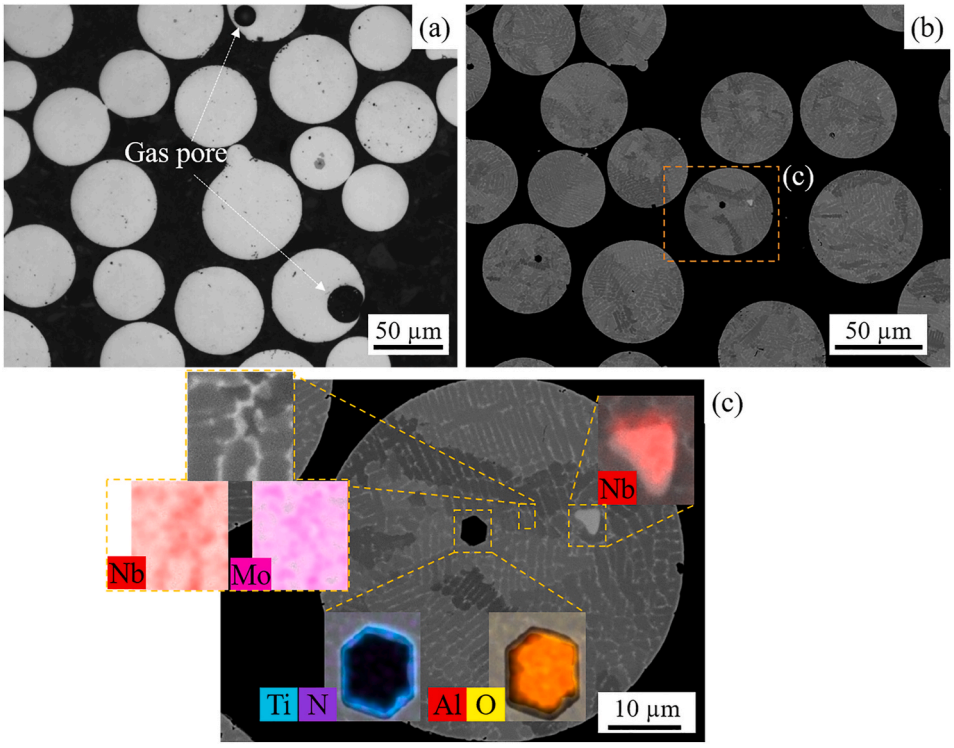

Fig. 1. (a) Optical and (b)–(c) scanning electron microscopy (SEM) micrographs with element maps (insets) of the cross-section of the Alloy 718 powder used in this study. A higher magnification SEM micrograph of Nb and Mo rich phase is also shown in the inset.

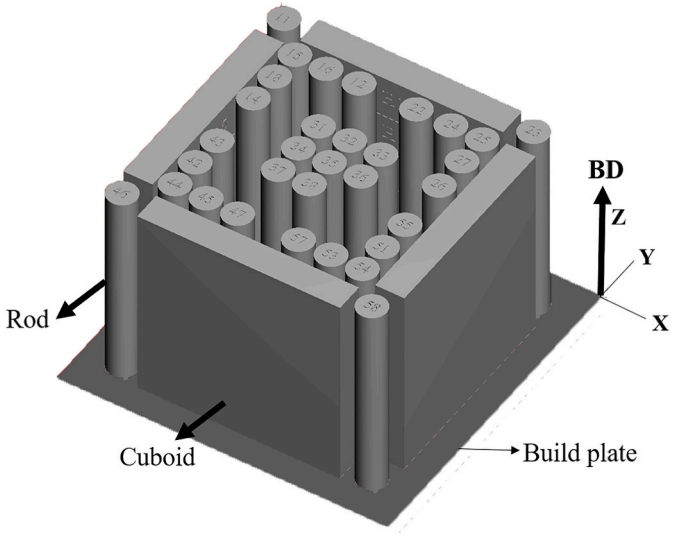

Fig. 2. CAD model of an EBM build; the arrow indicates the build direction (BD). Three such builds were studied in this work.

Table 2
Hatch process parameters used for the three EBM Alloy 718 builds.

Parameters	Settings for the three EBM builds	
	Build I/II	*Build III*
Melting strategy	bi-directional raster	Uni-directional raster
Melt current range (mA)	3.5–18	2.5–15
Speed function	63	94
Focus offset (mA)	15	7.5
Layer thickness (μm)	75	70
Hatch rotation (°)	72	63
Line off-set (μm)	125	120
Voltage (kV)	60	60
Pre-heat temperature (°C)	1020	1000

aging which is typically applied to EBM Alloy 718. Such an effort involving study of microstructure evolution during each step can potentially provide insight into possibility of shortening the duration of HT. Therefore, through this work, we aim to understand how the post-treatment protocol can be shortened specifically for EBM-built Alloy 718 through an in-depth investigation of microstructure as well as the resulting mechanical response under static and cyclic loading conditions.

2. Experimental procedure

2.1. EBM processing of Alloy 718

The plasma wire atomized Alloy 718 powder used in the present study was provided by AP&C (Montréal, Canada) with composition as given in Table 1. The nominal powder size in the range of 45–106 μm as provided by the supplier was also confirmed using image analysis employing a particle analyser (ABC model, IST AG, Switzerland). The powder cross-sections appeared circular with presence of few satellites, as shown in Fig. 1 (a) and (b). Moreover, few gas pores were also observed as shown in Fig. 1 (a). The source of gas pores is primarily expected to be the argon gas used during the powder atomization process [29]. Phases rich in Nb, presumably carbides and Laves phase, were also observed as shown in Fig. 1 (c), where the latter is also rich in Mo. Given that the nitrogen and oxygen content in the powder (refer Table 1) exceeds the solubility limit in Alloy 718 [30], some amount of TiN and Al_2O_3 inclusions, respectively were also expectedly found. These inclusions could have formed during powder production and could have

Table 3
Designations and details of the post-treatments.

Designation	Post-treatment details	Remarks
HIP	1120 °C, 100 MPa, 4 h, RC (390 °C/min)	Lower temperature bound as per ASTM F3055 [11]. Further variants with lower duration were also performed.
ST	954 °C, varying durations (15 min, 30 min, 45 min, 60 min), WC	As per ASTM F3055 and also commonly used for δ phase precipitation [36]
Age1	740 °C, varying durations (1 h, 4 h, 8 h), AC	Aging temperatures were middle point of those specified in ASTM F3055 (Age1: 720 °C/760 °C and Age2: 620 °C/650 °C)
Age1+Age2	740 °C, 8 h, FC at 55 °C/h to 635 °C, held at 635 °C for varying durations (1 h, 4 h, 8 h), followed by AC	
Age (4 h + 1 h)	740 °C, 4 h, FC at 55 °C/h to 635 °C, held at 635 °C for 1 h, AC	Further variants were also performed, such as Age (5 h + 1 h) and Age (6 h + 1 h)
HIP + HT*	1120 °C, 100 MPa, 4 h, RC (390 °C/min) to 160 °C; 954 °C, 100 MPa, 1 h, RC (350 °C/min) to 160 °C; 740 °C, 85 MPa, 4 h, cooled at 55 °C/h to 635 °C, held at 635 °C, 80 MPa for 1 h, followed by RC (310 °C/min)	Note that high pressure was maintained throughout the combined cycle.

Note- RC: rapidly cooled, FC: furnace cooled, AC: air cooled and WC: water cooled.

also come directly from the wire used for atomization [31]. Moreover, due to recycling, the powder could have undergone further oxidation because of prior exposure to EBM processing [32,33].

The Alloy 718 powder was processed using Arcam A2X EBM machines to make cuboids (100 × 100 × 15 mm) and cylinders (100 × 15 mm) as illustrated in the CAD model of a build shown in Fig. 2. One such build was supplied by Arcam AB (Mölndal, Sweden), henceforth referred to as *Build I*. An additional build was produced using similar process parameters at University West (Trollhättan, Sweden) which is henceforth referred to as *Build II*. Microstructurally both these builds were found to be nearly identical. The builds were produced using stainless steel base plates, and the key EBM process parameters are listed in Table 2. It should be mentioned that since the present study focuses exclusively on the hatch region, only the hatch melting parameters have been specified. However, it should be noted that contour melting, using spot melting, was employed which comprised 1–2 mm of the exterior of the specimens. More details pertaining to the contour region can be found in Ref. [34]. A third build, named *Build III*, similar in geometry as the build shown in Fig. 2 was also supplied by Arcam AB, with some key process parameters varied as stated in Table 2. For construction of all the three EBM builds, the automatic mode was kept on. The *Build I* was comprehensively investigated and unless specified otherwise all the stated results correspond to this build. The *Build II* (produced using similar process parameters as *Build I*) was used mainly for extracting more mechanical test specimens. Lastly, the *Build III* was constructed to study the influence of a different starting microstructure and to also investigate the robustness of the shortened thermal post-treatment protocol developed as an outcome of the microstructural evolution investigation carried out as part of this work.

2.2. Post-treatments

Parts of the EBM builds were subjected to several post-treatments as given in Table 3. The basis for selection of the parameters was ASTM F3055 standard for powder bed fusion built Alloy 718 [11]. The HIP treatments were performed at Quintus Technologies AB (Västerås, Sweden) in a hot isostatic press (Model QIH21, Quintus Technologies, Sweden) with a molybdenum furnace and argon was used as the inert process gas. The employed low HIPing temperature has been earlier

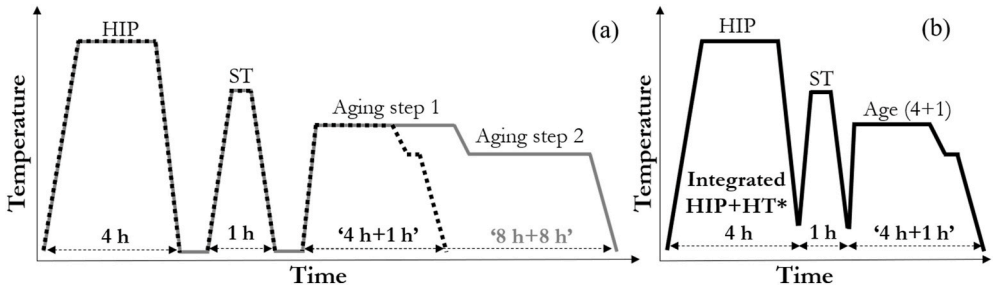

Fig. 3. Illustration of (a) conventional (grey solid line) and shortened (black dotted line) post-treatments for EBM Alloy 718 investigated in this work; (b) integrated shortened post-treatment HIP + HT* performed inside the HIP vessel. More details stated in Table 3.

metallographically shown to be effective in closing defects even in builds where large amounts of defects were intentionally introduced in the as-built condition [35]. The HTs (ST and aging) were carried out in an alumina tube furnace (model R120/500/13, Nabertherm GmbH, Germany) in inert argon atmosphere. For study of microstructure evolution during the recommended durations for ST and aging, to look for opportunity to shorten these steps, the hold time during each of these treatments was systematically varied as given in Table 3. The holding time was counted right after inserting the specimen into the furnace pre-heated to the required holding temperature. The investigated post-treatments are also schematically shown in Fig. 3 (a). Another approach for performing post-treatment is to integrate the HIP and HT and carry it out as a single uninterrupted cycle inside the HIP vessel. One such integrated cycle, designated HIP + HT*, was performed as given in Table 3 and illustrated in Fig. 3 (b).

2.3. Material characterization

For microstructure analysis, sections from the middle region of the cuboid specimens (see Fig. 2) in as-built and post-treated conditions were taken. All the sectioned specimens were hot mounted in a conductive polymer and metallographically prepared with a final polish using 0.05 μm silica suspension. For visualization of grain size, no etching was required; however, for subsequent characterization of carbides, electrolytic etching using Oxalic acid solution in water (1:10) was used with 2–3 V applied for 3–10 s. Specifically for characterization of γ"/γ′ and δ phase through SEM, a modified etching procedure was developed. A diluted solution of Kalling's 2 reagent in ethanol (1:1) was used with 2–3 V applied for 3–5 s. Specimens for transmission electron microscopy (TEM) analysis were prepared by manually grinding 500 μm thick wafers down to a thickness of 110–120 μm using SiC papers. Discs of 3 mm diameter were punched out and were further ground to a 100 μm thickness before subjecting to dimple grinding to ~50 μm thickness using a Gatan Model 656 dimple grinder. This was followed by electropolishing in a 10:90 methanol:perchloric acid solution at −40 °C using a Struers Tenupol-3 twinjet electropolisher until a hole was detected in each specimen.

Microscopy was performed using an Olympus BX60 M (HOFSTRAgroup®, US) OM device, three different SEM devices (HITACHI TM3000, Japan, LEO 1550 Gemini and Gemini 450, Zeiss, Germany), and a FEI Talos F200X (Thermo Scientific™, US) TEM device. To get better channelling contrast for visualization of grains, SEM analysis was carried out using lower acceleration voltage of 5 kV, whereas for other purposes it was set to 15 or 20 kV. The TEM analysis was performed using acceleration voltage of 200 kV. For electron backscattered diffraction (EBSD) analysis an HKL Nordlys EBSD detector from Oxford Instruments was used. Brightfield and darkfield imaging, selected area electron diffraction (SAED), and energy-dispersive X-ray spectroscopy (EDS) were performed. The SAED and EDS were specifically carried out for identification of secondary particles in the analysed specimens.

For quantification of defects and carbide content, at least ten OM and SEM micrographs, respectively, were analysed in each case at appropriate magnification to get representative values as recommended in the ASTM E1245-03 automatic image analysis method [37]. The micrographs were subjected to image analysis using ImageJ software and the average and 95% confidence interval values were evaluated as suggested in the above ASTM standard. For defect analysis samples were characterized prior to etching. During carbide analysis, to avoid noise during image analysis of these bright particles, bright features smaller than 160 nm in diameter were not considered. Quantification of size of γ" phase particles was conducted using manual image analysis of TEM darkfield images generated using the same zone axis [001] and same SAED spots (refer Fig. 4) for samples in different conditions to enable reliable comparison. For each analysed sample condition, over 50 precipitates were analysed for quantification of length and thickness of the particles as previously done by Chang et al. [38]. High resolution SEM analysis was also employed to visualize the γ"/γ′ precipitates.

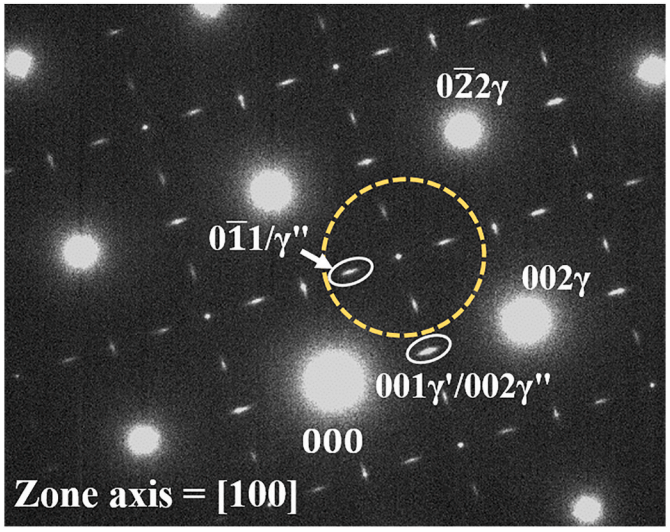

Fig. 4. A representative SAED pattern with the encircled (using yellow dotted line) superlattice reflections used for generating the darkfield micrographs.

2.4. Mechanical testing

Vickers microhardness testing using a Shimadzu HMV-2 (Japan) microhardness tester was performed and for each indent a load of 0.5 kgf was applied for 15s. All the tests were performed on polished specimens and, for each specimen, 15 indents were recorded. Tensile tests were also performed along the build direction for specimens in selected conditions. The tensile specimens were machined to a round dog-bone type geometry designed according to ASTM E8 [39] with a parallel length of 50 mm and a circular cross-section of diameter 6.3 mm. The tests were performed, following the above ASTM standard, at room temperature in strain-controlled mode using a Zwick/Roell Z100 (Zwick

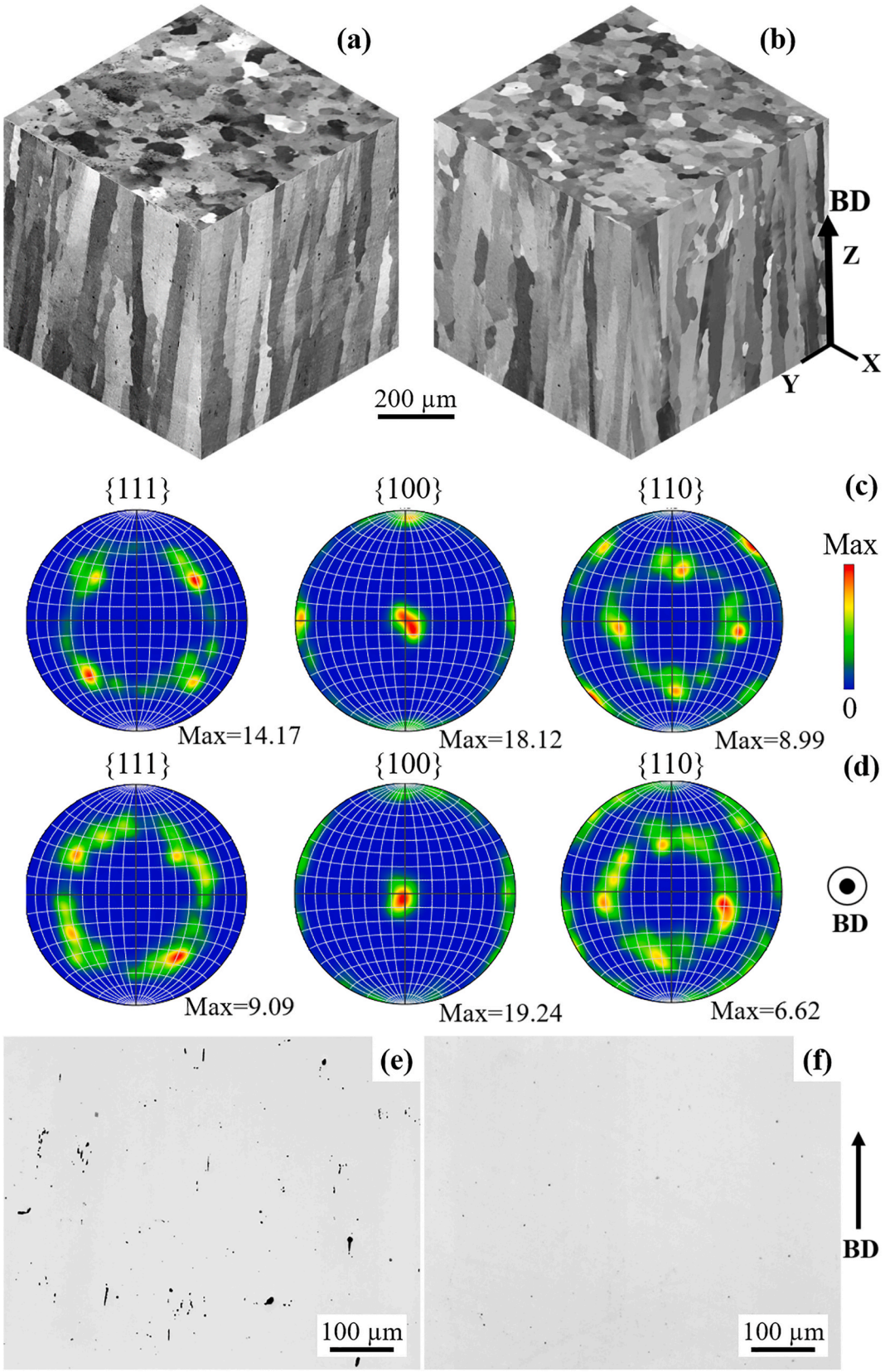

Fig. 5. 3D construction of SEM micrographs showing grain structure and pole figures (equal area projections) for (a), (c) as-built and (b), (d) HIPed condition. OM micrographs showing defects in (e) as-built and (f) HIPed specimens (*Build I*). The arrow and the encircled dot indicate the build direction.

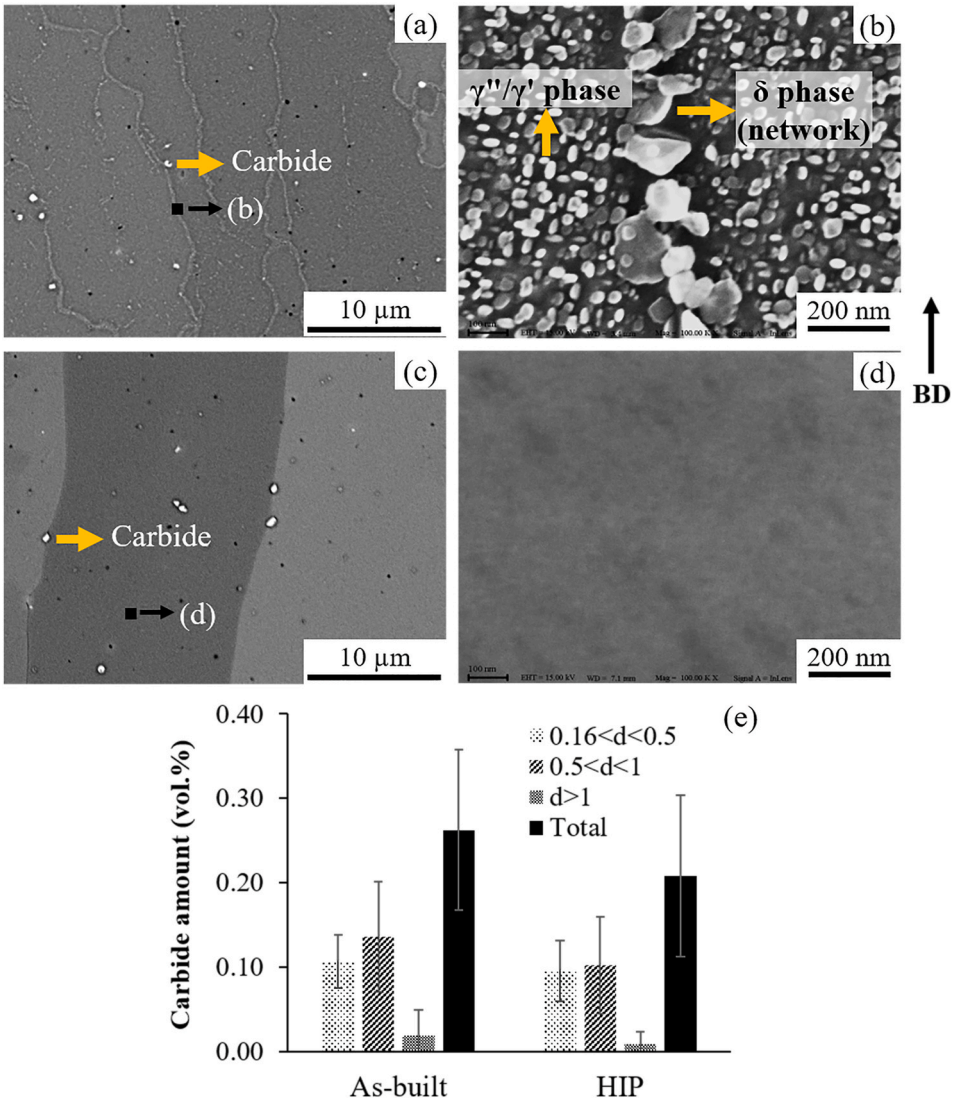

Fig. 6. SEM micrographs revealing secondary phases present in (a)–(b) as-built and (c)–(d) HIPed specimen; note the absence of δ and γ''/γ′ phases in (d). Carbide content in as-built and HIPed specimens, evaluated through image analysis with size distribution in terms of diameter 'd' in μm, depicted in (e) (*Build I*). The arrow indicates the build direction.

Roell Group, Ulm, Germany) machine. The tests were conducted using a clip-on extensometer for accurate determination of Young's modulus and yield strength of the material. The values for percentage elongation at fracture and ultimate tensile strength were evaluated from global measurements. A minimum of three specimens were tested in each condition and the average and standard deviation in the values was evaluated.

Low cycle fatigue (LCF) testing of selected specimens was also conducted along the build direction in push-pull mode. The fatigue specimens were machined to a round dog-bone type geometry with a parallel length of 19 mm and a circular cross-section of diameter 6.35 mm. The tests were performed at GKN Aerospace AB (Sweden) in ambient room conditions using an MTS 810 load frame (Minnesota, USA) equipped with a TestStar IIs servo-hydraulic closed loop control system operated in stress-controlled mode with $R = 0$ ($\Delta\varepsilon_{compression} = 0$). The specimens were tested at two stress amplitudes, i.e., 800 MPa and 900 MPa, and the corresponding number of tests performed for each sample condition were, two and one, respectively.

3. Results and discussion

Consistent with the main goal of the present study, the effect of each steps associated with post-treatment, namely HIPing, ST and two-step aging, on the microstructure and mechanical behaviour of EBM Alloy 718 was comprehensively investigated. Evolution of microstructure during ST and two-step aging was also comprehensively investigated. The outcome of the above was then utilized to conceive a shortened post-treatment protocol and the ensuing results, for both microstructure and mechanical properties, were compared with those from a 'standard' post-treatment schedule recommended as per ASTMF3055 [11]. The prominent findings are elaborated below.

3.1. Effect of HIPing

The as-built material as shown in Fig. 5 (a) mainly consisted of columnar grains with length typically of the order of a millimetre and width in the range of 10–100 μm. The latter was measured on the transverse cross-section by line intercept method, as the long columnar grains along the build direction appear rather equiaxed in transverse direction (see Fig. 5 (a)). The grains exhibited a very strong {100}

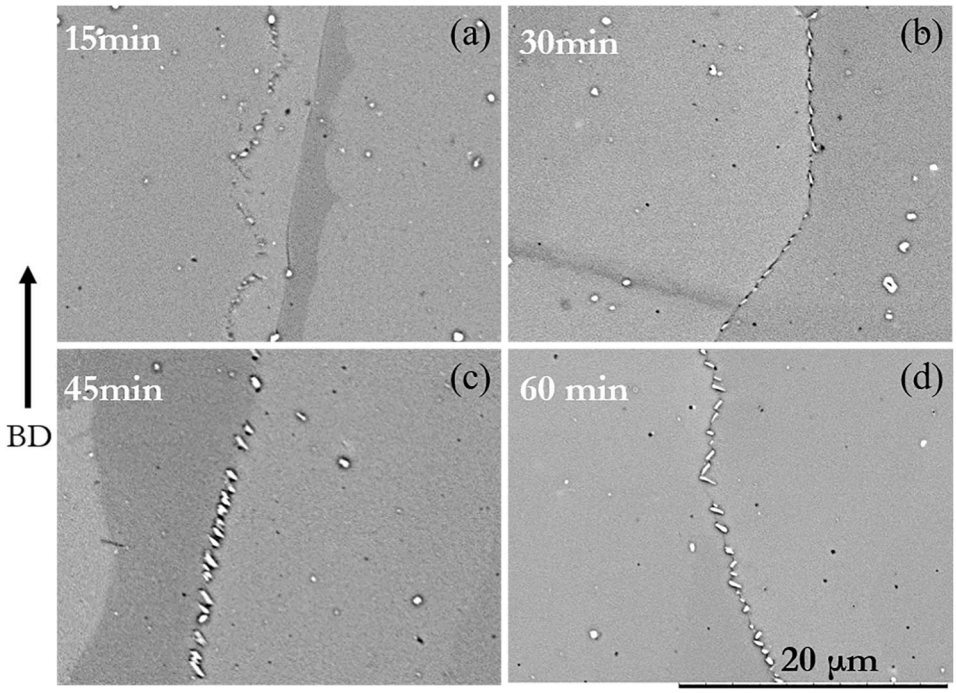

Fig. 7. SEM micrographs showing evolution of δ phase with the indicated varied ST times for prior-HIPed specimen (a)–(d). The arrow indicates the build direction.

texture along the building direction (refer Fig. 5 (c)). This is rationalized by <100> being the fastest growing direction in case of materials with face centred cubic crystal structure. This strong orientation dependence is commonly observed in EBM Alloy 718 [6]. The {111}, {100}, {110} pole figures for the as-built and HIPed material given in Fig. 5 (c) and (d) reveal that the {100} texture along the build direction was retained after the HIP treatment. Moreover, after HIPing no evident grain growth was observed (refer Fig. 5 (b)). This could be understood by the low HIPing temperature (1120 °C), as HIPing at higher temperature, which is commonly used for AM Alloy 718, has been shown to lead to grain growth [9,40].

From the above it can be seen that for microstructure analysis of EBM Alloy 718, the XZ plane (or YZ plane, along build direction) is representative because it provides information along several layers of the build, and both the grain width and length can be clearly discerned. Moreover, due to the symmetric nature of the process (particularly due to beam rotation during hatch melting) the microstructure in XZ and YZ planes appear to be similar. Further microstructure investigation was carried out along the XZ/YZ plane.

The as-built material contained three kinds of defects, i.e. gas porosity, shrinkage porosity and lack of fusion. After HIPing, the defects were reduced from 0.15% in the as-built condition to 0.02%, which is also seen in Fig. 5 (e) and (f). The remnant defects after HIPing were either gas pores or those associated with inclusions. These results reaffirm prior studies reporting gas porosity [41] and inclusions filled defects, both inherited from the powder (refer Fig. 1), retained after HIPing [5,35]. The HIPing treatment also promoted homogenization of the material. The δ phase particles, with plate-like morphology, present in the as-built condition and seen as bright network at low magnification (refer Fig. 6 (a) and (b)) were dissolved after HIPing. This is due to the HIPing temperature being above the δ solvus (982 °C–1037 °C [42]) and application of fast cooling in the present case (refer Table 3) after holding at HIPing temperature inhibited re-precipitation. Similarly, the strengthening precipitates (γ″/γ′ phases), which have even lower solvus temperature (below ~900 °C [42,43]), were also dissolved during HIPing. However, quantitatively no effect on the carbide content and size was observed after HIPing (refer Fig. 6 (e)), as its dissolution temperature (~1250 °C [31,44]) is above the HIPing temperature (1120 °C). These Nb-rich carbide particles were also confirmed using SAED and EDS analysis during TEM investigation. It may also be pointed out that the carbide particles can be beneficial for limiting grain growth in Alloy 718 through pinning the grain boundaries at high temperatures [45].

Given the relatively larger body of information available on conventional cast Alloy 718, which inspire the post-treatment protocols for AM Alloy 718, it is educative to evaluate how the above response of AM builds compares with previously reported results for cast material. A study also employing low temperature for HIPing (1120 °C) of Alloy 718 casting showed complete defect closure, although some Nb-rich segregations, particularly Laves phase, were retained after HIPing [13]. Such inhomogeneity in the cast material even after HIPing could explain the usual choice of higher temperature for HIPing (1150 °C or 1200 °C) commonly employed [9,40].

3.2. *Microstructural evolution during solution treatment*

Subjecting the EBM Alloy 718 to sub-solvus ST led to precipitation of δ phase at the grain boundaries, regardless of whether prior HIPing was used or not. The δ phase particles, which were noted to have precipitated during the first 15 min of ST, appeared to grow with time for nearly the entire 1 h duration of ST as shown for a prior-HIPed sample in Fig. 7. Similar evolution of δ phase during ST was also observed when the samples were not subjected to any prior HIPing treatment, although not shown herein for the sake of brevity. However, the samples subjected to prior HIPing appeared to exhibit lower amount of δ phase overall. This could be attributed to increased homogenization as a consequence of HIPing, since the equilibrium volume fraction and the precipitation kinetics for δ phase are reported to increase with increase in chemical segregation [46]. Irrespective of whether or not prior HIPing was performed, the δ phase particles formed during ST were not uniformly present at all grain boundaries. This could be explained by the previously observed preferential formation of δ phase at high angle grain boundaries during ST of EBM Alloy 718 [6]. Given that the δ phase is incoherent with the matrix, its precipitation particularly at the high angle grain boundaries is energetically favourable [47].

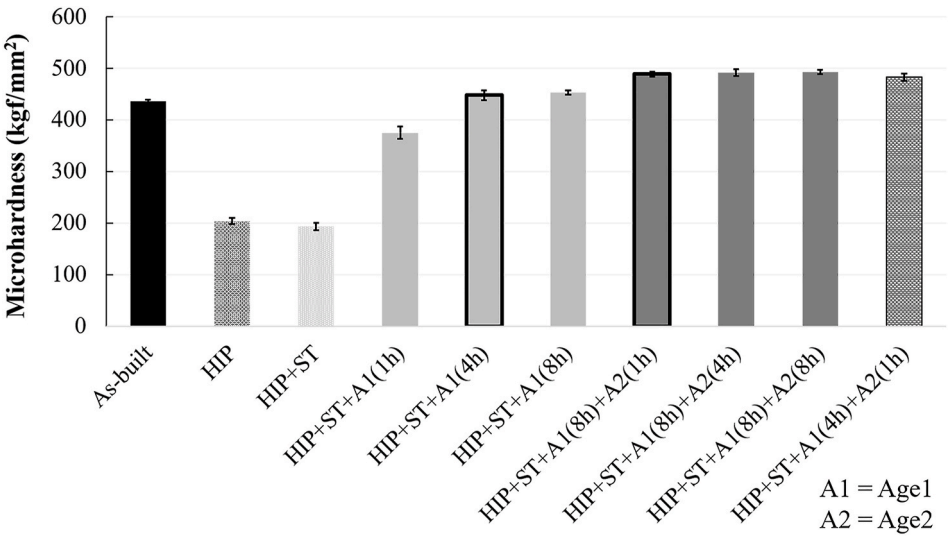

Fig. 8. Variation of microhardness during post-treatment (*Build I*).

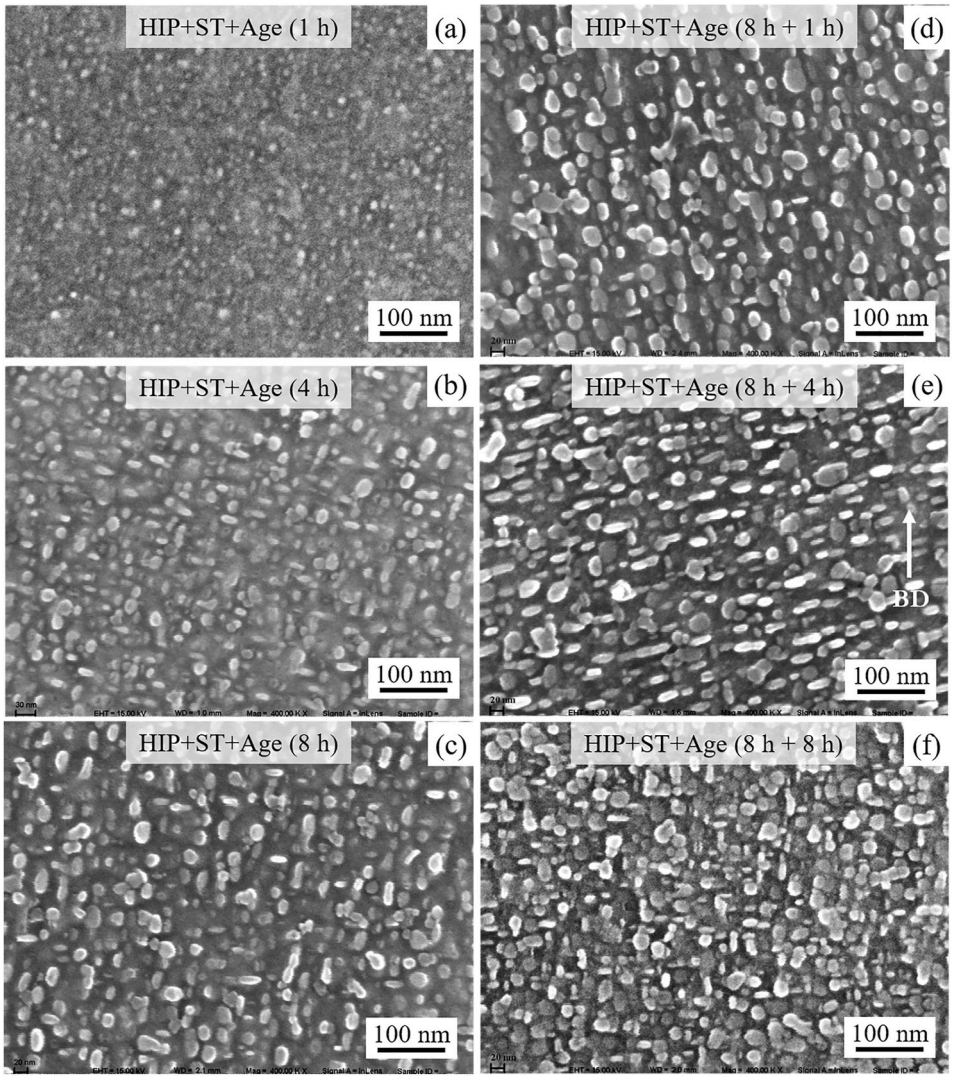

Fig. 9. High-magnification SEM micrographs of aged HIP + ST specimens showing evolution of strengthening precipitates during Age1 after (a) 1 h, (b) 4 h, (c) 8 h, and following Age1 (8 h) +Age2 treatments: (d) 8 h + 1 h, (e) 8 h + 4 h, (f) 8 h + 8 h (*Build I*). The arrow indicates the build direction.

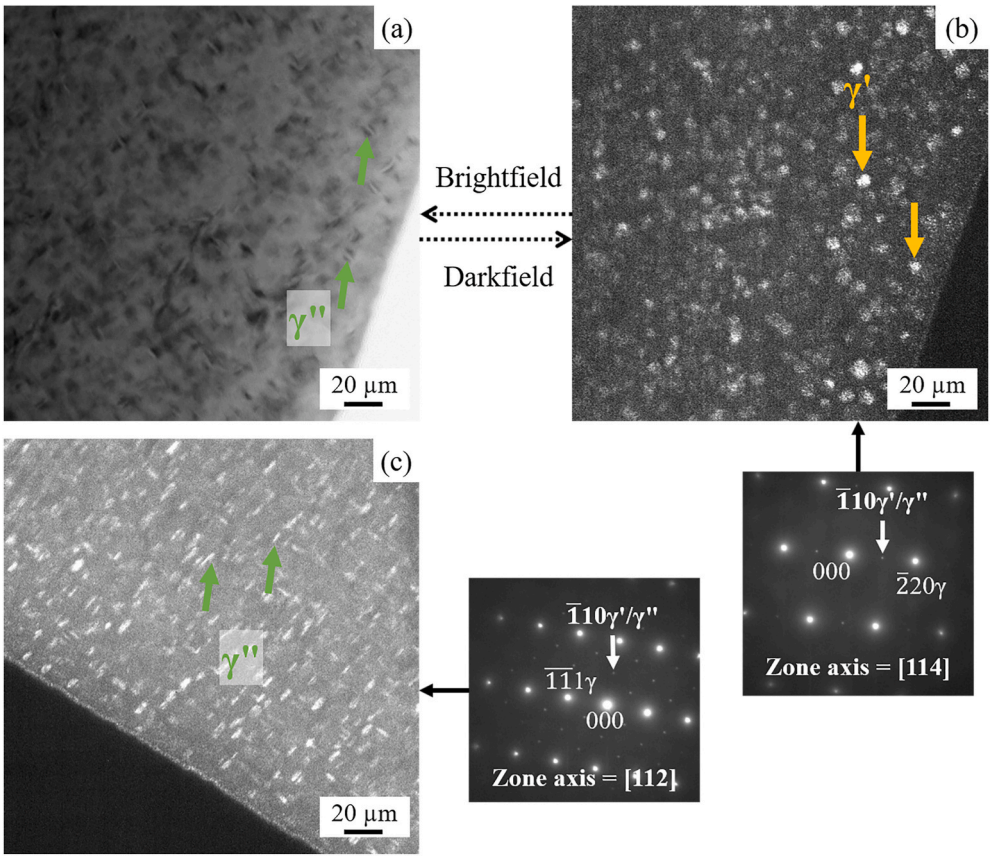

Fig. 10. Bright- and darkfield TEM micrographs of the same region of HIP + ST specimen subjected to Age1 for 1 h, to distinguish γ" and γ′ phases (a)–(b). Darkfield image showing γ" phase particles in the same specimen (c). The corresponding SAED patterns are also given with indicated superlattice diffraction spots which were used for generating the corresponding darkfield images (*Build I*).

3.3. *Microstructural evolution during aging*

The aging treatment was performed for precipitation of the strengthening phases. The evolution of these phases during aging was first indirectly gauged using hardness as the response, since precipitation of the strengthening γ"/γ′ phases is expected to have a strong correlation with the hardness of the material. Such an approach has also been previously adopted to study the effect of different aging temperatures and durations on LPBF [48] and wrought [23,49] Alloy 718. Furthermore, Jackson et al. [50] have reported a positive correlation between the hardness and strength of a precipitation hardened nickel-based superalloy.

The noted change in hardness with each of the post-treatment steps is depicted in Fig. 8. The hardness was reduced to the 'intrinsic' hardness of the matrix (~200 kgf/mm^2) after the HIPing treatment (1120 °C, 4 h, 100 MPa). This is as expected since HIPing caused complete dissolution of the strengthening precipitates, with the fast cooling (>300 °C/min) after holding preventing any noticeable re-precipitation, also shown in Fig. 6 (d). This finding is consistent with the noted absence of strengthening phases in wrought Alloy 718 after subjecting to temperature of 1100 °C for 1 h followed by cooling at 50 °C/min [51]. After HIPing, application of subsequent ST had no evident effect on the hardness, as it did not cause precipitation of strengthening phases. However, subjecting the specimens to aging treatment led to increase in hardness. During the course of first step of aging (Age1), the hardness was observed to increase with increasing aging duration from 1 h to 4 h, but further continued holding at Age1 temperature led to no evident effect on the hardness. However, after the additional second stage of aging (Age2), a jump in hardness was observed after 1 h, i.e. after 8 h + 1 h. Prolonged holding at Age2 led to no significant change in hardness. Therefore, the hardness appears to flatten after 4 h of Age1 and also after 1 h of Age2.

The hardness observations were further supported by results from high-magnification SEM imaging of the strengthening precipitates provided in Fig. 9 (a)-(f). After 1 h of Age1 treatment, the precipitates were too small to be effectively visualized using SEM. Therefore, TEM imaging was also performed and the results are provided in Fig. 10, which clearly shows precipitation of both γ" and γ′ phases after 1 h of Age1. Further it can be evidently seen from the comparison of the micrographs in Fig. 9 (a) and (b) that, after 1 h of Age1 the precipitates grew during the 4 h of treatment. However, qualitatively there is no noticeable effect of additional aging beyond 4 h during Age1 (i.e. 8 h in total as recommended in the ASTM F3055 standard [11]) as observed from the micrographs. With application of Age2 for 1 h, further growth of precipitates can be seen in Fig. 9 (d). As in case of Age1, with further prolonged duration of Age2 beyond 1 h, qualitatively, no evident effect on the precipitates could be discerned. Thus, the above hardness and microstructure observations are indicative of a possibility to shorten the duration for the traditional two-step aging treatment from the usual Age (8 h + 8 h) cycle to perhaps a trimmed Age (4 h + 1 h) cycle.

After subjecting the material to Age (4 h+ 1 h) treatment with prior HIP + ST, the hardness was in the range of 470–480 kgf/mm^2. This value is close to 490 kgf/mm^2 obtained after Age (8 h + 8 h) with prior HIP + ST. This similarity in hardness was also reflected in the microstructure after Age (4 h + 1 h) and Age (8 h + 8 h) treatments with prior HIP + ST, as shown in Fig. 11. Further, quantitative comparison of the frequency-size plot for the major strengthening phase γ" given in Fig. 12 shows reasonably similar precipitate distribution after Age (4 h + 1 h) treatment as after the standard Age (8 h + 8 h) treatment.

During direct aging of wrought Alloy 718, recent study by Theska

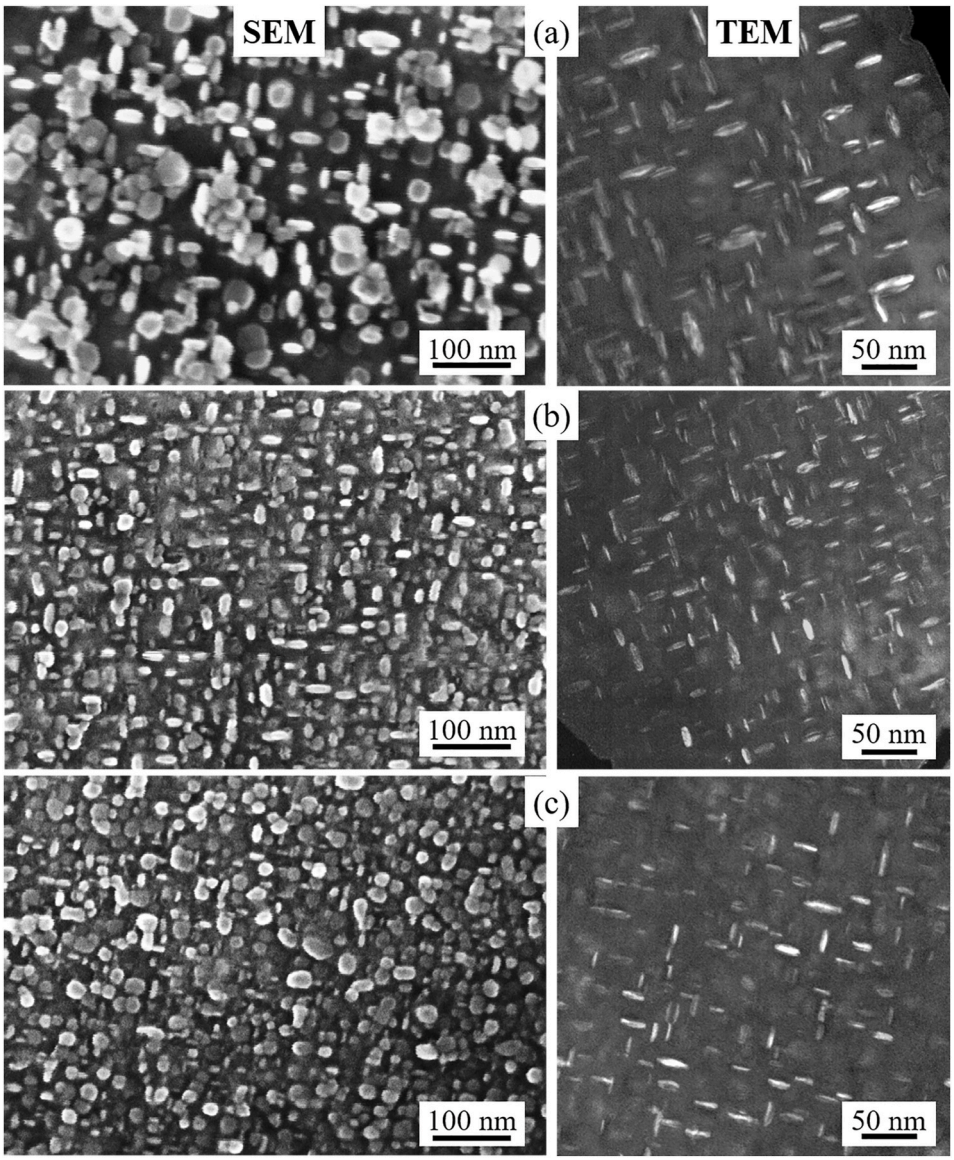

Fig. 11. SEM micrographs and TEM darkfield micrographs for (a) as-built, (b) HIP + ST + Age (4 h + 1 h) and (c) HIP + ST + Age (8 h+ 8 h) samples.

et al. [52] observed plateauing of hardness during Age1 (at 720 °C) after 4.5 h and noted a jump in hardness after application of Age2 treatment. McAllister et al. [53] observed increased number density of γ"-γ′ co-precipitates after transition from Age1 to Age2. Increased nucleation of strengthening precipitates was also found to cause increased hardness in wrought Alloy 718 [14]. Contrary to the above, Slama et al. [22] observed decrease in hardness after holding at 750 °C beyond 4 h. However at 760 °C, Fisk et al. [14] reported plateauing of hardness after ~5 h (to ~8 h) of holding. Thus, from the above it can be inferred that the precipitation characteristics of strengthening precipitates is very sensitive to the starting microstructure as also earlier noted by Thompson et al. [27] and Kumara et al. [28]. This is also further reflected in distinctly varied time-temperature-transformation curves reported for Alloy 718 [27,28,54,55].

Interestingly, overall the precipitates were finer and more populous after post-treatment compared to those in the as-built condition, as evident from Fig. 12, and this could have contributed to the observed higher hardness after post-treatment as shown in Fig. 8. In other words, the aging treatment significantly contributed to increased hardness through increase in precipitation strengthening of the material. This can be understood as follows. The extent of coherency strain hardening by the precipitates, particularly of γ" phase, can change with change of their size. Recent findings by Theska et al. [52] propose coherency loss of γ" particles above length of 38 nm and aspect ratio $\geq$ 3.3. Devaux et al. [56] also proposed loss of coherency of γ" particles beyond length of ~40 nm. It can be seen from Fig. 12 that considerable fraction of the analysed particles in as-built condition were above 40 nm in length compared to significantly finer particles sizes observed after post-treatment. In the context of size of precipitates, another interesting observation which is not often reported in the literature for Alloy 718 is the presence of large γ′ particles which are comparable to the length of γ" particles seen after aging (refer Figs. 10 and 13). In HT:ed LPBF built Alloy 718, the size of γ′ and γ" was comparable [57]. Whereas the large body of literature on wrought Alloy 718 reported typically smaller size of the γ′ phase compared to the γ" phase after aging [22,58]. The reason for the large size of γ′ precipitates observed in AM Alloy 718 needs further investigation.

3.4. Mechanical property evaluation with shortened post-treatments

As a logical follow-up to the preceding microstructure evolution study that suggested a potential to shrink the post-treatment schedule,

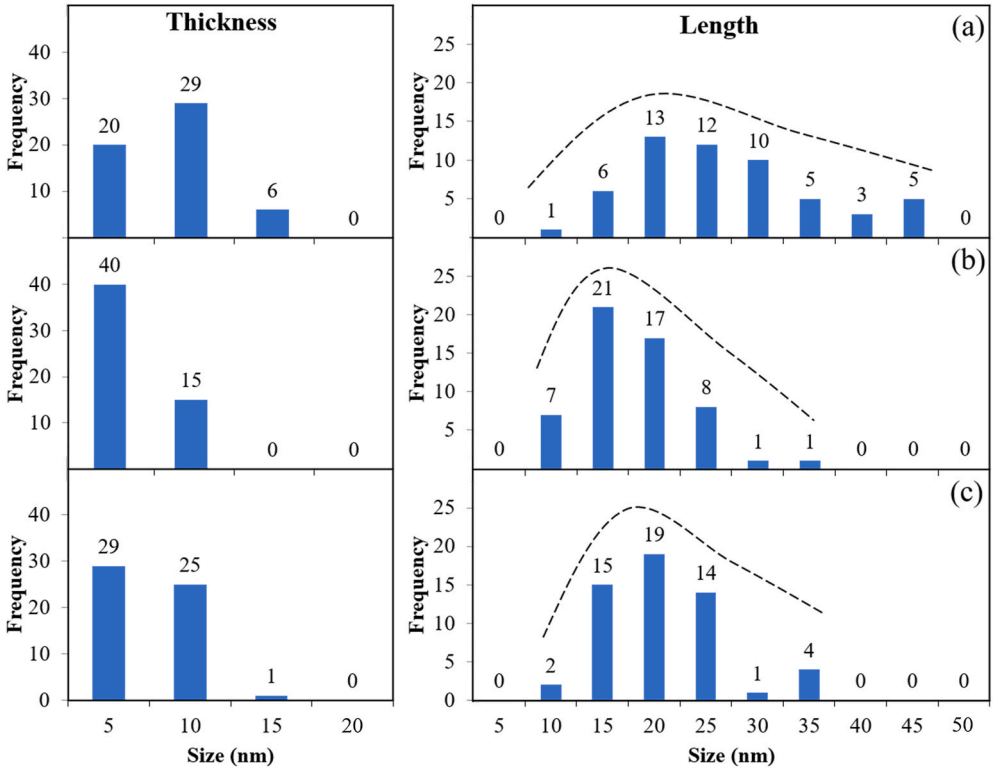

Fig. 12. Quantitative estimation of the thickness and length of the γ" phase particles evaluated using TEM darkfield micrographs for (a) as-built, (b) HIP + ST + Age (4 h + 1 h) and (c) HIP + ST + Age (8 h + 8 h) samples (*Build I*).

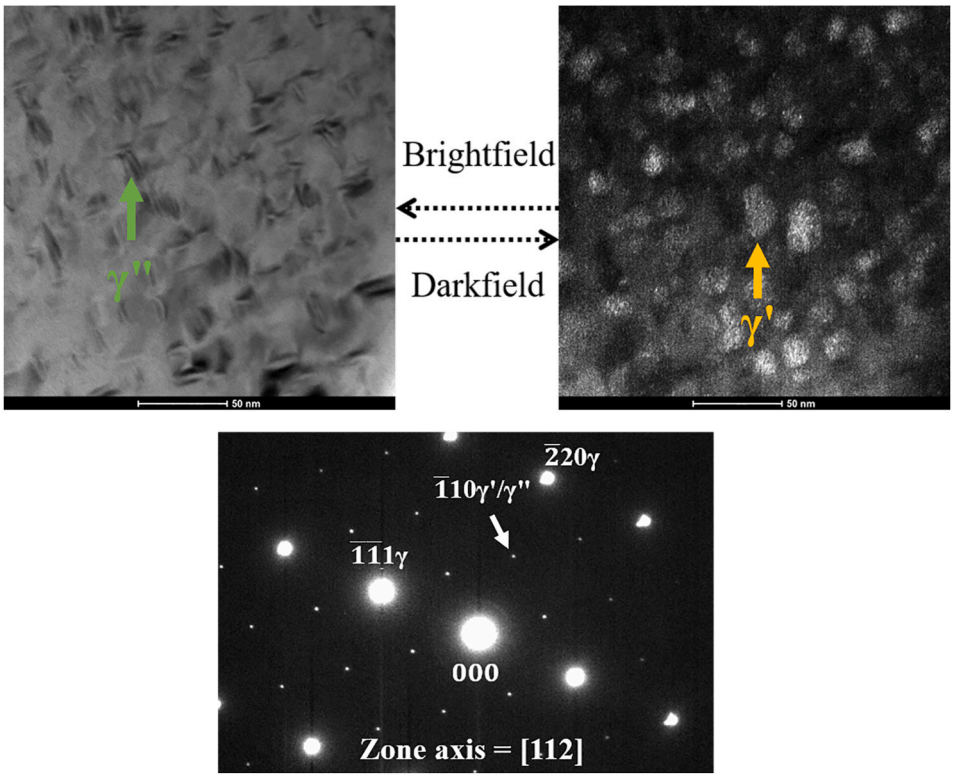

Fig. 13. Bright- and darkfield TEM micrographs from the same region showing the presence of γ′ and γ'' particles of comparable size after HIP + ST + Age (4 h+ 1 h); corresponding SAED pattern with indicated superlattice reflections used for generating the darkfield micrographs is also provided (*Build I*).

Table 4
Room temperature tensile behaviour of EBM Alloy 718 in as-built and various post-treated conditions; standard specification for wrought and cast material also provided for reference. Here YS, UTS and E and El_r stand for yield strength, ultimate tensile strength, Young's modulus and elongation to rupture, respectively.

EBM *Build*	Sample condition	YS (MPa)	UTS (MPa)	E (GPa)	El_r (%)
I	As-built	915 ± 7	1139 ± 23	127 ± 6	18 ± 4
II	As-built	931 ± 1	1113 ± 21	129 ± 5	25
III	As-built	920 ± 9	1177 ± 6	143 ± 3	17 ± 2
II	Age (4 h+ 1 h)	1051 ± 2	1232 ± 16	124 ± 2	21 ± 0
I	ST+Age (4 h + 1 h)	1093 ± 10	1228 ± 10	127 ± 1	18 ± 1
II	HIP+Age (4 h + 1 h)	1080 ± 0	1160 ± 0	128 ± 3	23 ± 4
I	HIP+ST+Age (4 h + 1 h)	1100 ± 0	1223 ± 6	129 ± 2	21 ± 1
II	HIP+ST+Age (4 h + 1 h)	1110 ± 10	1190 ± 0	131 ± 2	21 ± 2
III	HIP+ST+Age (4 h + 1 h)	1088 ± 12	1250 ± 6	144 ± 1	13 ± 1
II	HIP+ST+Age (6 h + 1 h)	1153 ± 32	1220 ± 10	122 ± 5	21 ± 2
II	HIP+ST+Age (8 h + 8 h)	1153 ± 40	1233 ± 12	127 ± 2	21 ± 1
II	HIP+HT*	1105 ± 6	1183 ± 3	127 ± 3	20 ± 1
	Wrought: Aerospace [57]	1034	1276, 1241	–	12, 10, 6
	Wrought: Oil and gas [58]	827–1000	1034	–	20
	Cast: Aerospace [59]	758	862	–	5

Table 5
LCF life (cycles to failure) for EBM Alloy 718 in as-built and post-treated conditions (*Build I*).

Stress amplitude	ST+Age (4 h+ 1 h)	ST+Age (8 h + 8 h)	HIP+ST+Age (4 h + 1 h)
800 MPa	$3*10^4$	$3.6*10^4$	$7*10^4$
800 MPa	$6.8*10^4$	$6.6*10^4$	$6.7*10^4$
900 MPa	$2.3*10^4$	$2.8*10^4$	$4.9*10^4$

mechanical property assessment was also taken up to validate the findings. The tensile behaviour and fatigue response results are summarized in Table 4 and Table 5, respectively. The HIPing treatment performed for 4 h caused defect reduction by an order of magnitude as shown earlier in Fig. 5 (f). However, the ductility of the EBM Alloy 718 investigated in this study was found to be not significantly influenced by HIPing, i.e., the material exhibited reasonably similar ductility in as-built and various post-treated conditions involving or excluding HIPing (see Table 4). A previous reported study had noted an increase in ductility of EBM Alloy 718 after subjecting to a post-treatment involving HIPing treatment [5]. Although the study did not report the defect content in the material, a possible explanation for the disparity in observations could be attributed to a possibly larger defect content in that study. This argument is further supported by the lower ductility of the sample in the as-built condition in the reported study (~10%) compared to the present study (~20%, *Build I*). Unlike the tensile behaviour, the fatigue response was significantly influenced by HIPing, as provided in Table 5. It can be seen from the table that, when HIPing was employed during post-treatment the LCF life values were significantly higher (with lower scatter) compared to the case when only long or short HT was performed. The improvement in LCF life after HIPing is attributable to closure of defects during HIPing. It is worth mentioning that EBM Alloy 718 in as-built condition was not subjected to fatigue test because of its relatively inferior mechanical properties as evidenced from the tensile behaviour provided in Table 4 as well as plotted in Fig. 14.

The effect of ST step, in a post-treatment cycle involving a subsequent aging treatment with or without prior HIPing, on the tensile behaviour of the material was also investigated. For this, as-built and HIPed samples were subjected to Age (4 h + 1 h) with or without prior ST. As evident from Table 4, only a marginal change in yield and/or ultimate tensile strength was observed whether or not ST was employed. This slight effect of ST could be due to small amount of δ phase precipitation during the ST applied in this study. When δ phase was present in small amounts (0.3–1.38 vol%), Valle et al. [59] reported no evident effect of δ phase on the tensile behaviour. However, when present in larger amount and depending on the nature of fracture during mechanical loading, the δ phase could significantly influence the mechanical response of the material. When fracture occurred through transgranular mode, Gopikrishna et al. [60] found that the δ phase present at the grain boundaries did not have any evident effect. However, when fracture happened through intergranular mode, Deng et al. [61] proposed the grain boundary δ phase to contribute to reduced intergranular cracking resistance. However, Yeh et al. [62] found increased creep rupture life when δ phase was present at the grain boundaries. This was attributed to the serrated grain boundary caused by δ phase precipitation as shown in Fig. 15 (a) and (b).

Subjecting as-built EBM Alloy 718 directly to aging (only Age (4 h + 1 h)) increased yield strength and ultimate tensile strength as compared to the as-built condition (see Table 4), but the tensile response appeared not to be significantly influenced whether or not the material was subjected to prior HIPing or ST. Therefore, out of all the post-treatment steps involving HIPing, ST and aging, only aging appeared to influence the tensile properties of EBM Alloy 718. From study of microstructure evolution during aging a possibility to shorten the treatment from the conventional Age (8 h + 8 h) cycle to a Age (4 h + 1 h) cycle was observed (refer Sec. 3.3). The microstructure observations were complemented by the comparable tensile response (refer Table 4). For easier comparison, the tensile results after these short and long post-treatments are also presented in Fig. 14. It can be seen that the yield strength and ultimate tensile strength differed by less than 5% in the two cases. Further variants of shortened aging were also investigated such as, Age (5 h + 1 h) and Age (6 h + 1 h) cycles. Although, the hardness after all these short aging treatments (Age (4 h + 1 h), Age (5 h + 1 h) and Age (6 h + 1 h)) was found to be similar to that after Age (8 h + 8 h), i.e. ~490 kgf/mm^2, the tensile strength was noted to be slightly higher after Age (6 h + 1 h) compared to Age (4 h + 1 h) treatment and nearly identical to the Age (8 h + 8 h) treatment as given in Table 4. These results demonstrate that the shortened aging treatment does not compromise in a notable way the tensile properties achieved following the post-treatment as specified in the ASTM standard.

To further assess the robustness of shorter aging, samples from *Build III*, which comprised of columnar and equiaxed grains were also subjected to HIP + ST + Age (4 h + 1 h) treatment. Application of such shortened post-treatment to *Build III* with finer grain structure (Fig. 16 (a) vs. Fig. 5 (a)) yielded increased tensile strength compared to the *Build I/II* (see Fig. 14). This implies that, apart from post-treatment, the as-built grain structure also has a strong influence on the mechanical behaviour of EBM Alloy 718. Although the strength was increased when grain size in the as-built condition was finer, the ductility was slightly reduced. For instance, after HIP + ST + Age (4 h + 1 h), the elongation in samples from *Build III* was 13% whereas it was 21% for samples from *Build I/II*. However, it should be noted, that the above values of ductility are still above the minimum requirements stated for cast or wrought Alloy 718 (refer Table 4). Sun et al. [63] have also reported low ductility in such EBM build (*Build III*) with fine columnar and equiaxed grains compared to build comprising of only coarser columnar grains (*Build I/II*). This was rationalized by the presence of unmelted/partially melted powder particles related to the equiaxed grains. This could be valid in

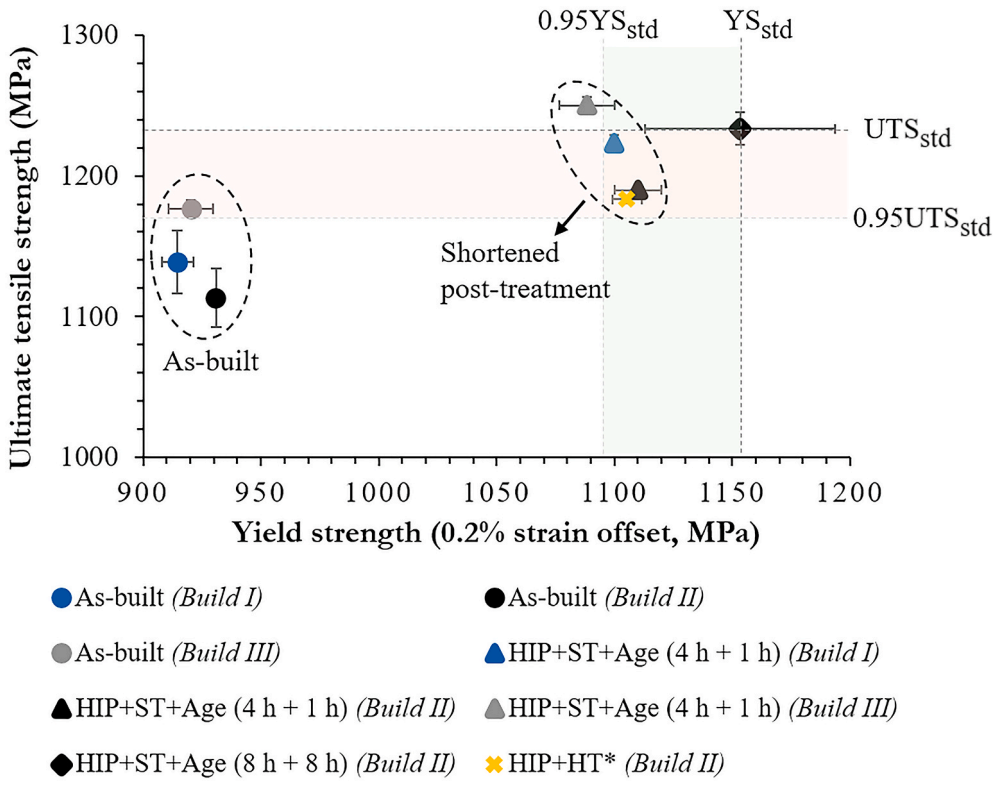

Fig. 14. Plot of ultimate tensile strength (UTS) vs. yield strength (YS) of EBM Alloy 718 in as-built and selected post-treated conditions. Here UTS$_{std}$ and YS$_{std}$ represent strength values obtained for the samples subjected to standard long post-treatment. Complete tensile property values for all the tested specimens is provided in Table 4.

the present case as the energy input during hatch melting was reduced for this build (*Build III*, refer Table 2). Lastly, for completeness it should be mentioned that the Young's modulus was not influenced by post-treatments applied in this study, however it was slightly altered with change in starting microstructure. Young's modulus was higher for the *Build III* (144 GPa) compared to the *Build I/II* (130 GPa), which could be rationalized by the reduced <100>//build direction texture in the former (Fig. 16 (c)) compared to the latter (Fig. 5 (c)). These results are corroborated by an earlier study on LPBF Alloy 718 where deviation from the <100>//build direction texture in the as-built condition was noted to yield increased Young's modulus [64]. In another study heat treatment was found to have no notable influence on the Young's modulus of LPBF Alloy 718 [65].

3.5. Integrating heat treatment with HIPing

Apart from reducing the time for aging as suggested by the preceding results, the post-treatment, involving HIPing, ST and aging, can be further shortened by integrating the various steps as a single uninterrupted cycle inside the HIP vessel. One such cycle HIP + HT*, involving HIP, ST, and Age (4 h + 1 h), as stated in Table 3 and schematically shown in Fig. 3 (b) was performed and the resultant tensile behaviour was similar to the material subjected to similar post-treatment cycles performed with conventional procedure of separate HIPing and HT, as shown in Fig. 14.

3.6. Further prospects for shortening the post-treatment protocol for EBM Alloy 718

3.6.1. Reduction in duration of HIPing

The observed improvement in LCF life after HIPing (see Table 5) is attributable to closure of defects during HIPing. The densification observed during the 4 h of HIPing at 1120 °C and 100 MPa was further found to be quantitatively similar after HIPing for lesser duration, i.e. 2 h or even 1 h at 1120 °C and 200 MPa. Thus, it appears that the time for HIPing can be potentially significantly reduced from the typical 4 h duration.

3.6.2. Possible elimination of solution treatment step

The sub-solvus ST applied in this study only caused precipitation of δ phase at the grain boundaries specifically when the EBM Alloy 718 was subjected to prior HIPing (see Fig. 7). Further, the tensile behaviour of EBM Alloy 718 was only marginal influenced by ST (refer Table 4). Therefore, in the context of shortening of post-treatment, a relevant concern could be the utility of ST in the entire post-treatment protocol consisting of HIPing and aging, as HIPing was also found to promote homogenization of the matrix.

4. Conclusion

In this study, the effect of various post-treatment steps (HIPing, solution treatment and aging) on the microstructure and mechanical behaviour of EBM built Alloy 718 was investigated. The conclusions drawn from the study are summarized below:

- HIPing at 1120 °C was found to cause significant order of magnitude reduction in defects. Due to the low temperature of HIPing, there was no noticeable impact on the grain size.
- During the sub-solvus solution treatment, the δ phase precipitated at the grain boundaries and was found to evolve for nearly the whole duration of the treatment irrespective of whether or not prior HIPing was performed. However, when prior HIPing was performed qualitatively reduced amount of δ phase was found which could be explained by increased homogenization during HIPing.
- The study of evolution of strengthening precipitates γ"/γ′ during aging suggested opportunity to substantially shorten the two-step

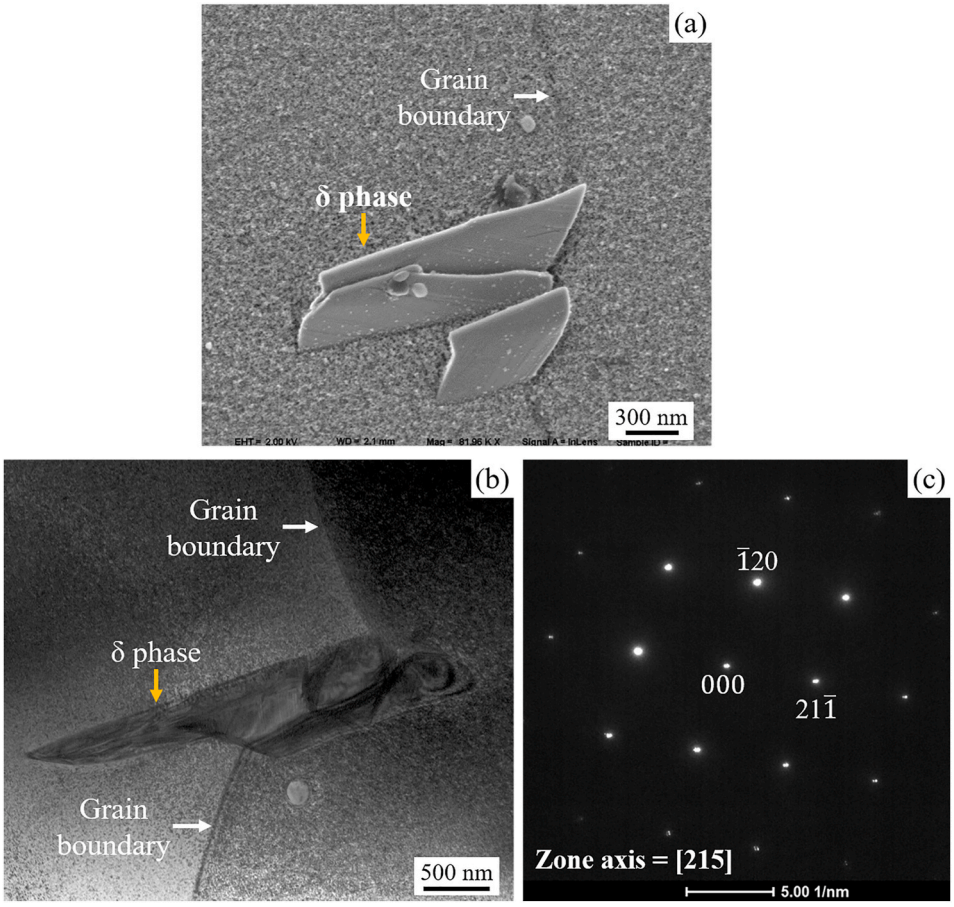

Fig. 15. High resolution (a) SEM micrograph and (b) TEM brightfield micrograph of δ phase at the grain boundary in a HIP + ST + Aged specimen (*Build I*). The δ phase was confirmed through SAED pattern given in (c).

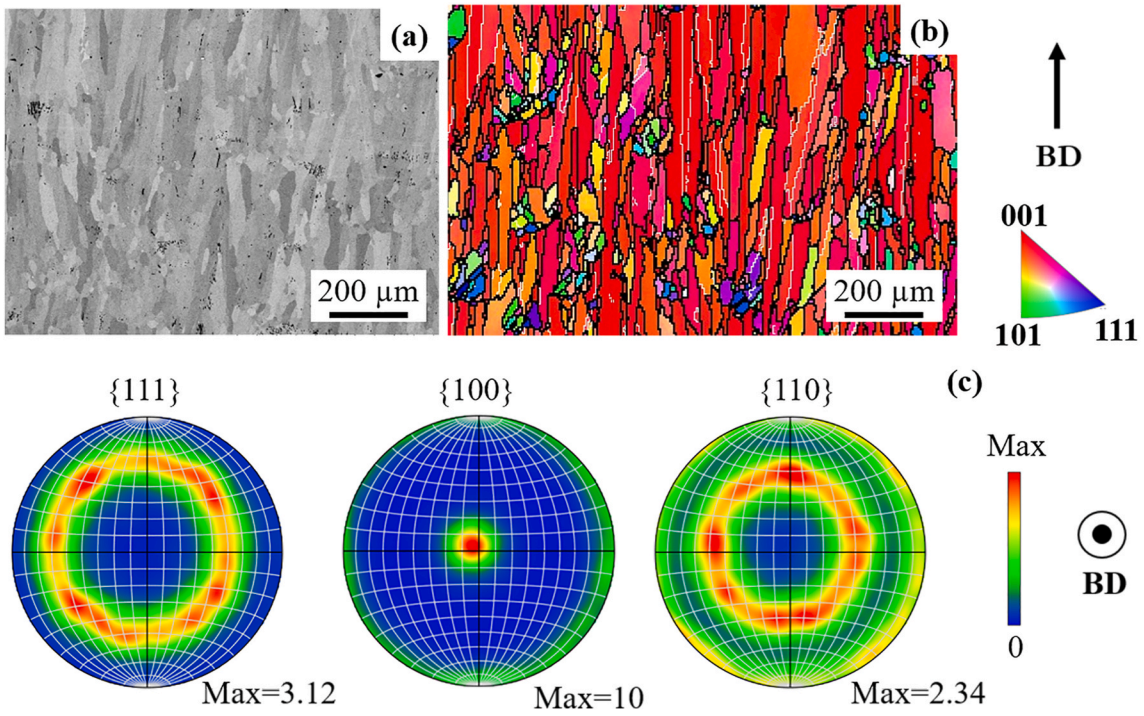

Fig. 16. (a) SEM micrograph and (b) EBSD orientation map of as-built specimen for *Build III* with (c) corresponding pole figures (equal area projection) mapped over reasonably large area using 5 μm step size. The orientation map is given in inverse pole figure colouring with respect to the build direction, and the colour code is provided. The arrow and the encircled dot indicate the build direction.

aging treatment to Age (4 h + 1 h) compared to the conventional long Age (8 h + 8 h) treatment developed for cast/wrought Alloy 718 but commonly applied to AM processed material.

- The tensile behaviour was found to be significantly influenced by the distribution of strengthening phases which were controlled through aging. While the fatigue behaviour was observed to depend on the presence of defects in the microstructure. Subjecting the material to HIPing treatment followed by heat treatment rendered significantly improved fatigue performance with additionally reduced scatter in values compared to the case when only HT was employed.
- The tensile response was not compromised by the shortened Age (4 h + 1 h) treatment. Moreover, the shortened post-treatment cycle involving HIPing, solution treatment and short aging was also successfully integrated inside the HIPing vessel to further reduce the entire duration of post-treatment.
- The presence of δ phase formed due to solution treatment had no evident effect on the tensile behaviour when aging was also employed. However, change in EBM process parameters can cause different as-built microstructures and affect tensile behaviour.
- There are further prospects for shortening the post-treatment protocol, such as (a) reducing HIPing time from 4 h to 1 h while increasing the pressure at a constant temperature, (b) possibility of skipping solution treatment particularly when the post-treatment protocol for EBM Alloy 718 is to involve HIPing treatment. Lastly, it should be mentioned that the findings from the present study can have significant techno-economic implications for how EBM Alloy 718 is post-treated.

Data availability

The raw/processed data required to reproduce these findings cannot be shared at this time due to technical or time limitations.

CRediT authorship contribution statement

Sneha Goel: Conceptualization, Methodology, Validation, Formal analysis, Investigation, Writing – original draft, Writing – review & editing, Visualization, Project administration. **Enrico Zaninelli:** Investigation, Writing – review & editing. **Tejas Gundgire:** Validation, Investigation. **Magnus Ahlfors:** Methodology, Investigation, Writing – Review. **Olanrewaju Ojo:** Methodology, Resources, Writing – review & editing, Project administration. **Uta Klement:** Methodology, Writing – review & editing, Supervision. **Shrikant Joshi:** Conceptualization, Methodology, Resources, Writing – review & editing, Supervision, Project administration, Funding acquisition.

Declaration of competing interest

The authors declare that they have no known competing financial interests or personal relationships that could have appeared to influence the work reported in this paper.

Acknowledgement

Financial assistance by the Knowledge Foundation through the SUMAN-Next project (20160281]) is gratefully acknowledged. The authors are grateful to Dr. Fouzi Bahbou and Dr. Niklas Israelsson from Arcam AB, Sweden for supplying the investigated material. Thanks to Mr. Jonas Olsson (University West, Sweden) for producing one of the EBM builds investigated in this study. Thanks to Mr. Johannes Gårdstam (Quintus Technologies AB, Sweden) for performing the HIPing treatments. The authors are also thankful to Dr. Abdul Khan (Manitoba Institute of Materials, Canada) for TEM characterization and analysis, and to Mr. Hamid Abedi (University of Manitoba, Canada) for assistance and guidance during TEM sample preparation. Assistance of Dr. Thomas Hansson and Mr. Jonas Kullgren (GKN Aerospace AB, Sweden) with fatigue testing is also acknowledged.

References

[1] Y. Zhao, K. Li, M. Gargani, W. Xiong, A comparative analysis of Inconel 718 made by additive manufacturing and suction casting: microstructure evolution in homogenization, Addit. Manuf. 36 (2020), https://doi.org/10.1016/j.addma.2020.101404.
[2] B. Wysocki, P. Maj, R. Sitek, J. Buhagiar, K. Kurzydłowski, W. Święszkowski, Laser and electron beam additive manufacturing methods of fabricating titanium bone implants, Appl. Sci. 7 (2017) 657, https://doi.org/10.3390/app7070657.
[3] C. Körner, Additive manufacturing of metallic components by selective electron beam melting — a review, Int. Mater. Rev. 61 (2016) 361–377, https://doi.org/10.1080/09506608.2016.1176289.
[4] L.E. Murr, Metallurgy of additive manufacturing: examples from electron beam melting, Addit. Manuf. 5 (2015) 40–53, https://doi.org/10.1016/j.addma.2014.12.002.
[5] A.R. Balachandramurthi, J. Moverare, S. Mahade, R. Pederson, Additive manufacturing of Alloy 718 via electron beam melting: effect of post-treatment on the microstructure and the mechanical properties, Materials (Basel) 12 (2018), https://doi.org/10.3390/ma12010068.
[6] D. Deng, J. Moverare, R.L. Peng, H. Söderberg, Microstructure and anisotropic mechanical properties of EBM manufactured Inconel 718 and effects of post heat treatments, Mater. Sci. Eng. 693 (2017) 151–163, https://doi.org/10.1016/j.msea.2017.03.085.
[7] K.A. Unocic, L.M. Kolbus, R.R. Dehoff, S.N. Dryepondt, B.A. Pint, High-temperature performance of UNS N07718 processed by additive manufacturing. NACE Corros, NACE International, San Antonio, USA, 2014. http://www.osti.gov/scitech/biblio/1132980.
[8] B. Shassere, D. Greeley, A. Okello, M. Kirka, P. Nandwana, R. Dehoff, Correlation of microstructure to creep response of hot isostatically pressed and aged electron beam melted Inconel 718, Metall. Mater. Trans. 49 (2018) 5107–5117, https://doi.org/10.1007/s11661-018-4812-z.
[9] P. Nandwana, M. Kirka, A. Okello, R. Dehoff, Electron beam melting of Inconel 718: effects of processing and post-processing, Mater. Sci. Technol. 34 (2018) 612–619, https://doi.org/10.1080/02670836.2018.1424379.
[10] J.K. Tien, T. Caulfield, Superalloys, Supercomposites, and Superceramics, Academic Press, New York, Boston, 1989.
[11] ASTM F3055−14a, Standard Specification for Additive Manufacturing Nickel Alloy (UNS N07718) with Powder Bed Fusion, ASTM Int., 2014, https://doi.org/10.1520/F3055-14A.
[12] N. El-Bagoury, T. Matsuba, K. Yamamoto, H. Miyahara, K. Ogi, Influence of heat treatment on the distribution of Ni2Nb and microsegregation in cast Inconel 718 alloy, Mater. Trans. 46 (2005) 2478–2483, https://doi.org/10.2320/matertrans.46.2478.
[13] P. Siereveld, J.F. Radavich, T. Kelly, G. Cole, R. Widmer, Effect of HIP parameters on fine grain cast Alloy 718, in: S. Reichman, D.N. Duhl, G. Maurer, S. Antolovich, C. Lund (Eds.), Superalloys, the Metallurgical Society, Champion, PA, USA, 1988, pp. 459–467, https://doi.org/10.7449/1988/Superalloys_1988_459_467.
[14] M. Fisk, J. Andersson, R. du Rietz, S. Haas, S. Hall, Precipitate evolution in the early stages of ageing in Inconel 718 investigated using small-angle x-ray scattering, Mater. Sci. Eng. 612 (2014) 202–207, https://doi.org/10.1016/j.msea.2014.06.036.
[15] F. Theska, A. Stanojevic, B. Oberwinkler, S.P. Ringer, S. Primig, On conventional versus direct ageing of Alloy 718, Acta Mater. 156 (2018) 116–124, https://doi.org/10.1016/j.actamat.2018.06.034.
[16] R. Schnitzer, S. Zinner, H. Leitner, Modeling of the yield strength of a stainless maraging steel, Scripta Mater. 62 (2010) 286–289, https://doi.org/10.1016/j.scriptamat.2009.11.020.
[17] O.R. Myhr, O. Grong, S.J. Andersen, Modelling of the age hardening behaviour of Al-Mg-Si alloys, Acta Mater. 49 (2001) 65–75, https://doi.org/10.1016/S1359-6454(00)00301-3.
[18] B. Oberwinkler, A. Fischersworring-Bunk, M. Hüller, M. Stockinger, Integrated process modeling for the mechanical properties optimization of direct aged alloy 718 engine disks, in: Proc. 13th Int. Symp. Superalloys, Minerals, Metals and Materials Society, Seven Springs, PA, USA, 2016, pp. 513–521, https://doi.org/10.1002/9781119075646.ch55.
[19] F.C. Campbell, Elements of Metallurgy and Engineering Alloys, ASM International, 2008.
[20] R.F. Decker, The evolution of wrought age-hardenable superalloys, J. Occup. Med. 58 (2006) 32–36, https://doi.org/10.1007/s11837-006-0079-8.
[21] M.C. Chaturvedi, Y. Han, Strengthening mechanisms in Inconel 718 superalloy, Met. Sci. 17 (1983) 145–149, https://doi.org/10.1179/030634583790421032.
[22] C. Slama, M. Abdellaoui, Structural characterization of the aged Inconel 718, J. Alloys Compd. 306 (2000) 277–284, https://doi.org/10.1016/S0925-8388(00)00789-1.
[23] K. Nakai, Y. Ohara, H. Ohtsubo, Y. Ohmori, Effects of lattice defect on pre-precipitation stages of γ' and γ" phases in a Ni-base superalloy, ISIJ Int. 36 (1996) 187–193, https://doi.org/10.2355/isijinternational.36.187.
[24] S. Azadian, Aspects of Precipitation in the Alloy Inconel 718, PhD Thesis, Luleå University of Technology, Sweden, 2004.
[25] W. Huang, J. Yang, H. Yang, G. Jing, Z. Wang, X. Zeng, Heat treatment of Inconel 718 produced by selective laser melting: microstructure and mechanical properties, Mater. Sci. Eng. 750 (2019) 98–107, https://doi.org/10.1016/j.msea.2019.02.046.

[26] D.D. Krueger, The development of direct age 718 for gas turbine engine disk applications. Superalloy 718, Metallurgy Appl., Pittsburgh, PA, USA, 1989, pp. 279–296, https://doi.org/10.7449/1989/SUPERALLOYS_1989_279_296.
[27] R.G. Thompson, J.R. Dobbs, D.E. Mayo, The effect of heat treatment on microfissuring in Alloy 718, Weld. J. 65 (1986) 299–304.
[28] C. Kumara, A. Segerstark, F. Hanning, N. Dixit, S. Joshi, J. Moverare, P. Nylén, Microstructure modelling of laser metal powder directed energy deposition of alloy 718, Addit. Manuf. 25 (2019) 357–364, https://doi.org/10.1016/j.addma.2018.11.024.
[29] J. Kroeger, F. Marion, Leading the way with plasma atomised Ti spherical powders for MIM, Powder Inject. Mould. Int. 5 (2011) 55–57.
[30] H. Helmer, Additive Fertigung durch Selektives Elektronenstrahlschmelzen der Nickelbasis Superlegierung IN718: Prozessfenster, Mikrostruktur und mechanische Eigenschaften, PhD Thesis, Friedrich-Alexander-Universität Erlangen-Nürnberg, Germany, 2016.
[31] H. Gruber, Electron Beam Melting of Alloy 718 Powder Recycling and its Effect on Defect Formation, Licentiate thesis, Chalmers University of Technology, Sweden, 2019.
[32] E. Hryha, R. Shvab, H. Gruber, A. Leicht, L. Nyborg, Surface oxide state on metal powder and its changes during additive manufacturing: an overview, Metall. Ital. (2018) 34–39.
[33] H. Gruber, M. Henriksson, E. Hryha, L. Nyborg, Effect of powder recycling in electron beam melting on the surface chemistry of Alloy 718 powder, Metall. Mater. Trans. 50A (2019) 4410–4422, https://doi.org/10.1007/s11661-019-05333-7.
[34] S. Goel, H. Mehtani, S.-W. Yao, I. Samajdar, U. Klement, S. Joshi, As-built and post-treated microstructures of an electron beam melting (EBM) produced nickel-based superalloy, Metall. Mater. Trans. 51 (2020) 6546–6559, https://doi.org/10.1007/s11661-020-06037-z.
[35] S. Goel, K. Bourreau, J. Olsson, U. Klement, S. Joshi, Can appropriate thermal post-treatment make defect content in as-built electron beam additively manufactured Alloy 718 irrelevant? Materials 13 (2020) 536, https://doi.org/10.3390/ma13030536.
[36] D. Dunyong, On the Microstructures and Anisotropic Mechanical Behaviours of Additively Manufactured IN718, PhD Thesis, Linköping University, Sweden, 2019.
[37] ASTM E1245-03, Standard practice for determining the inclusion or second-phase constituent content of metals by automatic image analysis, ASTM Int., 2008, pp. 1–8, https://doi.org/10.1520/E1245-03R16.
[38] L. Chang, W. Sun, Y. Cui, F. Zhang, R. Yang, Effect of heat treatment on microstructure and mechanical properties of the hot-isostatic-pressed Inconel 718 powder compact, J. Alloys Compd. 590 (2014) 227–232, https://doi.org/10.1016/j.jallcom.2013.12.107.
[39] ASTM E8/E8M, Standard test methods for tension testing of metallic materials, ASTM Int., 2010, pp. 1–11, https://doi.org/10.1520/E0008.
[40] W. Tillmann, C. Schaak, J. Nellesen, M. Schaper, M.E. Aydinöz, K.-P. Hoyer, Hot isostatic pressing of IN718 components manufactured by selective laser melting, Addit. Manuf. 13 (2017) 93–102, https://doi.org/10.1016/j.addma.2016.11.006.
[41] W.J. Sames, F. Medina, W.H. Peter, S.S. Babu, R.R. Dehoff, Effect of process control and powder quality on Inconel 718 produced using electron beam melting, in: 8th Int. Symp. Superalloy 718 Deriv. 2014, the Minerals, Metals & Materials Society, Pittsburgh, PA, USA, 2014, pp. 409–423, https://doi.org/10.1002/9781119016854.ch32.
[42] A.K. Koul, P. Au, N. Bellinger, R. Thamburaj, W. Wallace, J.-P. Immarigeon, Development of a damage tolerant microstructure for Inconel 718 turbine disc material, in: S. Reichman, D.N. Duhl (Eds.), Superalloys, the Metallurgical Society, Champion, PA, USA, 1988, pp. 3–12, https://doi.org/10.7449/1988/Superalloys_1988_3_12.
[43] Y. Ji, Y. Lou, M. Qu, J.D. Rowatt, F. Zhang, T.W. Simpson, L.-Q. Chen, Predicting coherency loss of γ" precipitates in IN718 superalloy, Metall. Mater. Trans. 47A (2016) 3235–3247, https://doi.org/10.1007/s11661-016-3480-0.
[44] A. Strondl, R. Fischer, G. Frommeyer, A. Schneider, Investigations of MX and γ'/γ" precipitates in the nickel-based superalloy 718 produced by electron beam melting, Mater. Sci. Eng. 480 (2008) 138–147, https://doi.org/10.1016/j.msea.2007.07.012.
[45] M.M. Kirka, Y.S. Lee, D.A. Greeley, A. Okello, M.J. Goin, M.T. Pearce, R.R. Dehoff, Strategy for texture management in metals additive manufacturing, J. Occup. Med. 69 (2017) 523–531, https://doi.org/10.1007/s11837-017-2264-3.
[46] C. Kumara, A.R. Balachandramurthi, S. Goel, F. Hanning, J. Moverare, Toward a better understanding of phase transformations in additive manufacturing of Alloy 718, Materialia 13 (2020), https://doi.org/10.1016/j.mtla.2020.100862.
[47] H. Zhang, C. Li, Q. Guo, Z. Ma, Y. Huang, H. Li, Y. Liu, Delta precipitation in wrought Inconel 718 alloy; the role of dynamic recrystallization, Mater. Char. 133 (2017) 138–145, https://doi.org/10.1016/j.matchar.2017.09.032.
[48] Y. Zhao, N. Sargent, K. Li, W. Xiong, A new high-throughput method using additive manufacturing for alloy design and heat treatment optimization, Materialia 13 (2020), https://doi.org/10.1016/j.mtla.2020.100835.
[49] J.J. Schirra, Effect of heat treatment variations on the hardness and mechanical properties of wrought inconel 718, in: E.A. Loria (Ed.), Superalloy 718, 625, 706, Var. Deriv., the Minerals, Metals and Materials Society, Pittsburgh, PA, USA, 1997, pp. 431–438, https://doi.org/10.7449/1997/Superalloys_1997_431_438.
[50] M.P. Jackson, R.C. Reed, Heat treatment of UDIMET 720Li: the effect of microstructure on properties, Mater. Sci. Eng. 259 (1999) 85–97, https://doi.org/10.1016/S0921-5093(98)00867-3.
[51] L. Geng, Y.-S. Na, N.-K. Park, Continuous cooling transformation behavior of Alloy 718, Mater. Lett. 30 (1997) 401–405, https://doi.org/10.1016/S0167-577X(96)00225-X.
[52] F. Theska, K. Nomoto, F. Godor, B. Oberwinkler, A. Stanojevic, S.P. Ringer, S. Primig, On the early stages of precipitation during direct ageing of Alloy 718, Acta Mater. 188 (2020) 492–503, https://doi.org/10.1016/j.actamat.2020.02.034.
[53] D. McAllister, D. Lv, L. Feng, H. Deutchman, A. Wessman, Y. Wang, M.J. Mills, Characterization and modeling of deformation mechanisms in Ni-base superalloy 718, in: Proc. 9th Int. Symp. Superalloy 718 Deriv. Energy, Aerospace, Ind. Appl, Springer International Publishing, 2018, pp. 319–338, https://doi.org/10.1007/978-3-319-89480-5_19.
[54] J.W. Brooks, P.J. Bridges, Metallurgical stability of inconel alloy 718, in: S. Reichman, D.N. Duhl, G. Maurer, S. Antolovich, C. Lun (Eds.), Superalloys, Minerals, Metals & Materials Society, 1988, pp. 33–42, https://doi.org/10.7449/1988/Superalloys_1988_33_42. Champion, USA.
[55] A. Oradei-Basile, J.F.F. Radavich, A current T-T-T diagram for wrought Alloy 718, in: Superalloys, Pittsburgh, PA, USA, 1991, pp. 325–335, https://doi.org/10.7449/1991/superalloys_1991_325_335.
[56] A. Devaux, L. Nazé, R. Molins, A. Pineau, A. Organista, J.Y.Y. Guédou, J.F. F. Uginet, P. Héritier, Gamma double prime precipitation kinetic in Alloy 718, Mater. Sci. Eng. 486 (2008) 117–122, https://doi.org/10.1016/J.MSEA.2007.08.046.
[57] L. Zhou, A. Mehta, B. McWilliams, K. Cho, Y. Sohn, Microstructure, precipitates and mechanical properties of powder bed fused inconel 718 before and after heat treatment, J. Mater. Sci. Technol. 35 (2019) 1153–1164, https://doi.org/10.1016/j.jmst.2018.12.006.
[58] M. Sundararaman, P. Mukhopadhyay, S. Banerjee, Some aspects of the precipitation of metastable intermetallic phases in INCONEL 718, Metall. Trans. A. 23A (1992) 2015–2028, https://doi.org/10.1007/BF02647549.
[59] L.C.M. Valle, L.S. Araújo, S.B. Gabriel, J. Dille, L.H. de Almeida, The effect of δ phase on the mechanical properties of an Inconel 718 superalloy, J. Mater. Eng. Perform. 22 (2013) 1512–1518, https://doi.org/10.1007/s11665-012-0433-7.
[60] D. Gopikrishna, S.N. Jha, L.N. Dash, Influence of microstructure on fatigue properties of Alloy 718, in: E.A. Loria (Ed.), Superalloy 718, 625, 706, Var. Deriv., the Minerals, Metals & Materials Society, Pittsburgh, PA, USA, 1997, pp. 567–573, https://doi.org/10.7449/1997/Superalloys_1997_567_573.
[61] D. Deng, R.L. Peng, J. Moverare, On the dwell-fatigue crack propagation behavior of a high strength superalloy manufactured by electron beam melting, Mater. Sci. Eng. 760 (2019) 448–457, https://doi.org/10.1016/j.msea.2019.06.013.
[62] A.C. Yeh, K.W. Lu, C.M. Kuo, H.Y. Bor, C.N. Wei, Effect of serrated grain boundaries on the creep property of Inconel 718 superalloy, Mater. Sci. Eng. 530 (2011) 525–529, https://doi.org/10.1016/j.msea.2011.10.014.
[63] S.-H. Sun, Y. Koizumi, T. Saito, K. Yamanaka, Y.-P.P. Li, Y. Cui, A. Chiba, Electron beam additive manufacturing of Inconel 718 alloy rods: impact of build direction on microstructure and high-temperature tensile properties, Addit. Manuf. 23 (2018) 457–470, https://doi.org/10.1016/j.addma.2018.08.017.
[64] V. Popovich, E. Borisov, A. Popovich, Vs Sufiiarov, D. Masaylo, L. Alzina, Functionally graded Inconel 718 processed by additive manufacturing: crystallographic texture, anisotropy of microstructure and mechanical properties, Mater. Des. 114 (2017) 441–449, https://doi.org/10.1016/j.matdes.2016.10.075.
[65] E. Chlebus, K. Gruber, B. Kuźnicka, J. Kurzac, T. Kurzynowski, Effect of heat treatment on microstructure and mechanical properties of Inconel 718 processed by selective laser melting, Mater. Sci. Eng. 639 (2015) 647–655, https://doi.org/10.1016/j.msea.2015.05.035.